



HAL
open science

Implementation of ‘chaotic’ advection for viscous fluids in heat exchanger/reactors

Zoé Anxionnaz-Minvielle, Patrice Tochon, Raphael Couturier, Clément
Magallon, Félicie Theron, Michel Cabassud, Christophe Gourdon

► **To cite this version:**

Zoé Anxionnaz-Minvielle, Patrice Tochon, Raphael Couturier, Clément Magallon, Félicie Theron, et al.. Implementation of ‘chaotic’ advection for viscous fluids in heat exchanger/reactors. *Chemical Engineering and Processing: Process Intensification*, 2016, 113, pp.118-127. 10.1016/j.cep.2016.07.010 . hal-01506812

HAL Id: hal-01506812

<https://hal.science/hal-01506812>

Submitted on 12 Apr 2017

HAL is a multi-disciplinary open access archive for the deposit and dissemination of scientific research documents, whether they are published or not. The documents may come from teaching and research institutions in France or abroad, or from public or private research centers.

L’archive ouverte pluridisciplinaire **HAL**, est destinée au dépôt et à la diffusion de documents scientifiques de niveau recherche, publiés ou non, émanant des établissements d’enseignement et de recherche français ou étrangers, des laboratoires publics ou privés.



Open Archive TOULOUSE Archive Ouverte (OATAO)

OATAO is an open access repository that collects the work of Toulouse researchers and makes it freely available over the web where possible.

This is an author-deposited version published in : <http://oatao.univ-toulouse.fr/>
Eprints ID : 17719

To link to this article : DOI: 10.1016/j.cep.2016.07.010
URL : <http://doi.org/10.1016/j.cep.2016.07.010>

To cite this version : Anxionnaz-Minvielle, Zoé and Tochon, Patrice and Couturier, Raphael and Magallon, Clément and Théron, Felicie and Cabassud, Michel and Gourdon, Christophe *Implementation of 'chaotic' advection for viscous fluids in heat exchanger/reactors.* (2016) Chemical Engineering and Processing: Process Intensification, 113. pp. 118-127. ISSN 0255-2701

Any correspondence concerning this service should be sent to the repository administrator: staff-oatao@listes-diff.inp-toulouse.fr

Implementation of ‘chaotic’ advection for viscous fluids in heat exchanger/reactors

Z. Anxionnaz-Minvielle^{a,*}, P. Tochon^a, R. Couturier^a, C. Magallon^a, F. Théron^b,
M. Cabassud^b, C. Gourdon^b

^a CEA, LITEN, DTBH, 17 rue des Martyrs 38054 Grenoble, France

^b University of Toulouse, Laboratoire de Génie Chimique UMR 5503 CNRS/INPT/UPS, 31432 Toulouse, France

A B S T R A C T

When viscous fluids are involved, laminar hydraulic conditions and heat and mass transfer intensification are conflicting phenomena. A channel geometry based on Split-And-Recombine (SAR) patterns is experimentally investigated. The principle implements the Baker’s transformation and ‘chaotic’ structures are generated to promote heat and mass transfer. This work assesses the energy efficiency of different heat exchanger/reactors integrating these SAR patterns.

The heat transfer capacity is assessed and compared with the energy consumption of each mock-up. It is sensitive to the cooling mode and to the number of SAR patterns per length unit as well.

The continuous oxidation of sodium thiosulfate with hydrogen peroxide has been implemented. Conversions up to 99% are reached according to the utility fluid temperature and the residence time.

Finally, the whole performances of the SAR geometries are compared to a plate-type heat exchanger/reactor with a corrugated pattern. The more viscous the fluid, the more the energy efficiency of the SAR design increases compared to the corrugated design because of the balance between advection and diffusion mechanisms. The interest in terms of energy efficiency in working with SAR heat exchanger/reactor appears from Reynolds numbers below 50.

Keywords:

Heat exchanger/reactor

Chaotic advection

Viscous fluids

Continuous mode

Process intensification

Split-And-Recombine pattern

1. Introduction

Among the technologies promoting process intensification [1,2], heat-exchanger/reactor (HEX reactor) is a promising one [3]. This device combines the benefits of a large heat transfer performance and a plug-flow regime allowing an intensive radial mixing, as a result of the specific design of process channels [4–9]. These geometries generate instabilities even in laminar flow regime ($50 < Re < 2000$). However most of the studies have been carried out with inviscid fluids and the intensification of performances when the fluid viscosity increases comes at the expense of pumping costs. Processes of food industry, intermediate chemistry like silicones or polymers, . . . involve viscous fluids and a study, carried out in the frame of the industrial network EUROPIC [10], pointed out that heat and mass transfers in viscous media are one of the main industrial concern. In the very laminar flow regime,

precluding turbulence as a mixing mechanism, mixing by diffusion can be efficient provided that the contact area is sufficient. This can be achieved with systems based on multi-lamination mechanism and baker’s transformation [11,12]. These have been proposed especially in the context of microfluidics [13–16]. In microfluidic devices, the typical channel dimensions and flow rates are so low that all flow is laminar ($Re \approx 0.1$) and turbulence cannot be achieved. Diffusion is also too slow to be effective requiring too long channel lengths. The implementation of viscous fluid streams in HEX reactor and the typical millimetre dimensions of the channel cross-section lead to similar conclusions. However, by applying a series of Baker’s transformations in dedicated three-dimensional mixing elements, named Split-And-Recombine (SAR) patterns, the required channel length can be reduced exponentially with the number of mixing patterns. The involved separation/stacking mechanisms lie on the Baker’s transformation principle. Two fluid streams are combined, split out-of-plane, rotated in opposite directions and recombined as illustrated with Fig. 1. Then, a 2-strips domain becomes 2^n alternating strips after n mixing patterns.

* Corresponding author.

E-mail address: zoe.minvielle@cea.fr (Z. Anxionnaz-Minvielle).

Nomenclature

| | |
|----------------|-----------------------------------------------------------------------|
| A | [m ²] heat exchange area |
| C_p | [J kg ⁻¹ K ⁻¹] thermal capacity |
| d_h | [m] hydraulic diameter |
| F_p | [kg h ⁻¹] process flowrate |
| F_u | [kg h ⁻¹] utility flowrate |
| L | [m] total length of the process channel |
| L_{dev} | [m] developed length of the process channel |
| \dot{n}_i | [mol s ⁻¹] initial molar flowrate |
| P_{loss} | [W] thermal loss |
| P_{th} | [W] thermal power |
| $P_{reaction}$ | [W] heat of reaction |
| Pe | [-] pecllet number (=Re Pr) |
| Pr | [-] prandtl number |
| Re | [-] reynolds number |
| T | [K] temperature |
| u | [m s ⁻¹] fluid velocity |
| U | [W m ⁻² K ⁻¹] global heat transfer coefficient |
| V | [m ³] volume of fluid |

Greek letters

| | |
|---------------|-----------------------------------------------------------|
| ΔH_r | [kJ mol ⁻¹] enthalpy of reaction |
| ΔP | [Pa] pressure drop |
| ε | [W m ⁻³] energy dissipation rate |
| Λ | [-] darcy coefficient |
| λ | [W m ⁻¹ K ⁻¹] thermal conductivity |
| μ | [Pa s] viscosity |
| ρ | [kg m ⁻³] density |
| χ | [%] conversion rate |

A very efficient mixing is achieved by diffusion and Schönfeld et al. [13] even proposed as an outlook to use similar SAR structures to improve heat transfer in mini heat exchangers. The influence of chaotic advection on heat transfer has been numerically and experimentally investigated [17–21]. Results in a single channel are promising.

The interest of HEX reactors is the close control of the reaction temperature. The very short characteristic lengths between both the process and the utility streams are of paramount importance. With three-dimensional SAR structures, characteristic dimensions are quite different from 'classical' two-dimensional patterns (plate-type HEX reactor) and heat transfer might be affected.

Thus to investigate the relevance of implementing SAR patterns in a HEX reactor device, performance indicators besides mixing have to be assessed. They account for heat transfer and energy consumption. The objective is to promote heat and mass transfer even in viscous conditions.

For that purpose, we experimentally characterized three stainless steel mock-ups –assembled by diffusion bonding. Two different flow patterns according to the number of SAR structures are considered. Their designs come from [14,15].

For one of these geometries, two cooling systems have been investigated, external cooling Plates –isothermal wall- and integrated cooling tubes. For each mock-up, the 3 mm square cross-section channels are around 3.5 m long. Then, a case study in reactive conditions is implemented with the continuous oxidation of sodium thiosulfate with hydrogen peroxide. Finally, the whole performances of the SAR geometries have been compared with the ones of a corrugated pattern plate-type heat exchanger/reactor [6].



Fig. 1. Illustration of a 3D mixing pattern. Top: Cross-section illustrating the Baker's transformation after two iterations. Bottom: sketch of mixing actions after two elements [11].

2. Heat-exchanger reactor design and integration

2.1. SAR patterns

Three SAR patterns, based on the designs of [14,15] have been considered. Fig. 2 depicts four patterns of each considered geometry.

The square cross-sections of the channels are 3 × 3 mm² corresponding to an equivalent hydraulic diameter of 3 mm. The Reynolds number assessment is based on this hydraulic diameter and on the fluid velocity at the inlet of the process channel, i.e. upstream the first fluid stream separation. This reference is taken since the inlet flowrate is a major process parameter for the industrial application.

Two channel lengths can be defined in the SAR geometries. We consider the developed length, L_{dev} and the total length, L . The former corresponds to the distance travelled by a single fluid particle between the inlet and the outlet of the HEX reactor. Whereas the latter corresponds to the sum of every stream branches, i.e. the total fluid volume divided by the cross section.

Patterns SAR-1 and SAR-2 are very similar. The difference stems from the pattern dimension on the z-axis when fluid stream is split. In comparison with SAR-2, the SAR-1 pattern is expanded to allow the insertion of cross-flow cooling tubes (see Section 2.2).

SAR-3 pattern is less complex than SAR-1 and SAR-2 patterns. It makes easier its manufacturing. It includes 3 bends per pattern versus 6 bends per pattern in both SAR-1 and SAR-2 geometries.

2.2. HEX reactor integration and manufacturing

The three SAR geometries are integrated in respectively three whole HEX reactor prototypes. To manufacture the HEX reactors, the SAR channel is first divided in several layers which are then transposed in corresponding plates as depicted in Fig. 3.

The HEX reactors are made of one process plate including several rows of SAR patterns in series and sensor connections at each end of the rows (see Fig. 4b).

The stratification step depicted in Fig. 3 is duplicated on the plate to obtain the required number of rows (see Fig. 4a). Laser machining is used and plates are then stacked into a container. The assembling process is based on diffusion bonding (High

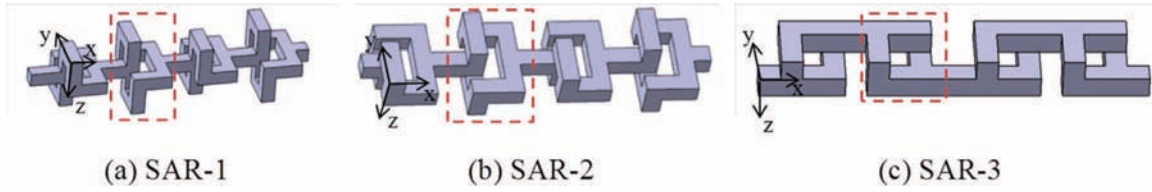


Fig. 2. SAR patterns. The red dotted lines delimit one SAR pattern. (For interpretation of the references to color in this figure legend, the reader is referred to the web version of this article.)

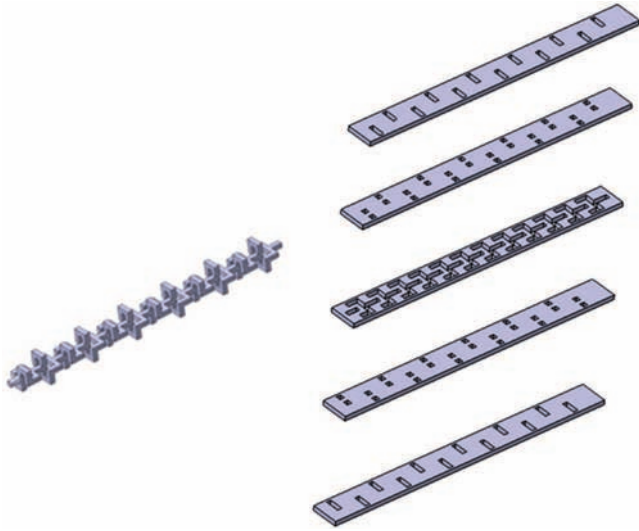


Fig. 3. Stratification of the SAR-2 pattern for the manufacturing process.

temperature Isostatic Pressing –HIP– assembling, [22]). The final prototype is made of stainless steel.

Two cooling configurations have been considered. The first one assumes isothermal wall temperature. The process plate (SAR-2 and SAR-3) is sandwiched between two cooling plates. The second cooling configuration involves cross-flow cooling tubes directly integrated through the SAR patterns (SAR-1). Fig. 5 illustrates SAR-1 and SAR-3 integration.

The final prototypes are around 185 mm long and 90 mm width. The geometrical characteristics are listed in Table 1.

2.3. Corrugated pattern

The performances of the previous SAR patterns are compared with a classical 2D corrugated one which design is based on the one studied by [5,6]. The manufacturing process of the 2D HEX reactor

is the same and the cooling system is based on isothermal walls (with cooling plates). The square cross-section of the corrugated channel is $2 \times 4 \text{ mm}^2$ and the hydraulic diameter is 2.67 mm. The channel is 2.2 m long including 103 bends (90°) per length unit. The corrugated channel is shown in Fig. 6.

3. Thermal and hydraulic investigations

To assess the HEX reactors performances, the studied Reynolds number ranges from 0.1 to 10,000. Water and two solutions of glycerol into water (70% w. and 90% w. of glycerol) are used.

3.1. Pressure drop

3.1.1. Experimental set-up and procedure

Pressure drops are measured with a differential pressure sensor between the inlet and the outlet of the HEX reactors. To cover a wide range of Reynolds number, distilled water, ethylene glycol and two solutions of glycerol are used (70% w. and 90% w.). The tests are implemented in isothermal conditions and the mean physico-chemical properties of the fluids are listed in Table 2. Since the temperature is measured during the pressure drop measurements, both the viscosity and the density are assessed at the exact test temperature.

From pressure drop measurements the Darcy coefficient, Λ , is assessed according to the following expression:

$$\Lambda = \frac{2 \cdot \Delta P \cdot d_h}{\rho \cdot L_{dev} \cdot u^2} \quad (1)$$

And the Reynolds number is defined as:

$$Re = \frac{\rho \cdot u \cdot d_h}{\mu} \quad (2)$$

where L_{dev} is the developed length of the process channel, and u the process fluid velocity. The SAR geometries are designed such as the pressure drops in each fluid branch are equal. Moreover, since a fluid particle flows successively through the inlet zone (flow velocity, u), a split branch (flow velocity, $u/2$), a stream

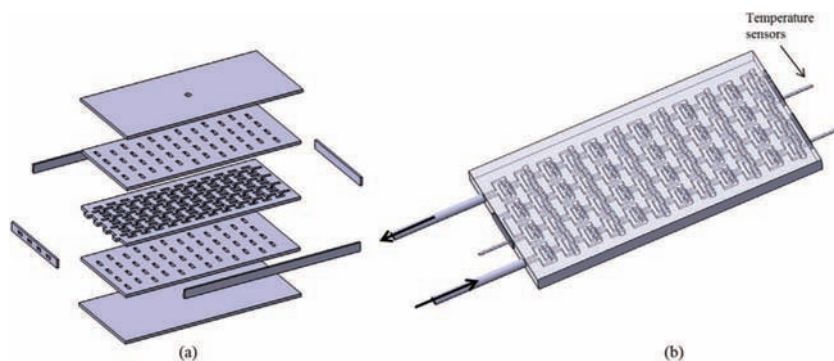


Fig. 4. Manufacturing steps for SAR-2 prototype– (a) Plates laser-machining, (b) Stacking.

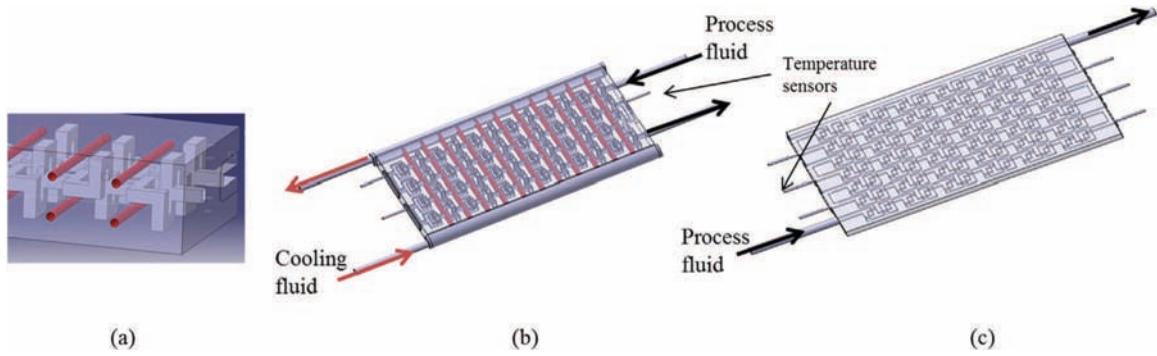


Fig. 5. CAD views of SAR-1 (a and b) and SAR-3 (c) HEX reactors. (a) Zoom of the crossing between the cooling tubes and the SAR-1 channel. (b) The cross-flow cooling tubes in SAR-1 HEX reactor are depicted in red.

Table 1
Geometrical characteristics of SAR HEX reactors.

| | SAR-1 | SAR-2 | SAR-3 |
|-------------------------------------------------|--------------------------|----------------------------------|----------------------------------|
| Cooling configuration | cross-flow cooling tubes | Cooling plates (isothermal wall) | Cooling plates (isothermal wall) |
| Cross-section (mm ²) | | 3 × 3 | |
| Hydraulic diameter (mm) | | 3 | |
| Developed length, L_{dev} (m) | 1.9 | 1.7 | 2.1 |
| Total length, L (m) | 3.4 | 2.8 | 3.4 |
| Total volume (mL) | 28.3 | 24.7 | 28.5 |
| Number of rows in series | 4 | 4 | 7 |
| Number of patterns per row | 12 | 12 | 12 |
| Number of patterns per unit of developed length | 25 | 29 | 39.5 |

recombination zone (flow velocity, u), a split branch (flow velocity, $u/2$), . . . We decided to consider the developed length to assess the Darcy coefficient in the SAR geometries.

3.1.2. Results and discussion

Fig. 7 shows the evolution of the Darcy coefficient with the Reynolds number in both the SAR and the corrugated channels.

No major discontinuity is observed between the glycerol 0.7w. curve (Reynolds number from 5 to 90) and the glycerol 0.9w. one

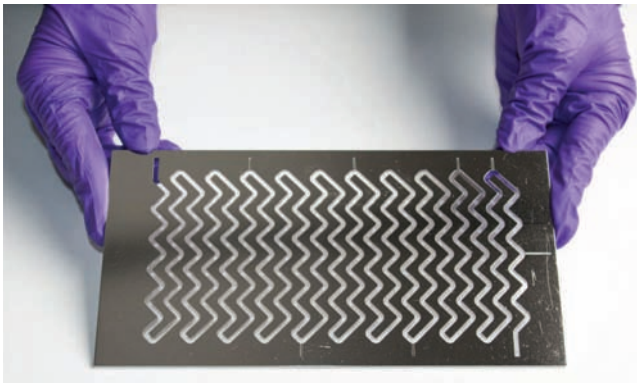


Fig. 6. Photograph of the corrugated channel before HIP assembling.

(Reynolds number from 0.1 to 3). Whatever the geometry, a linear sharp decrease is observed as for straight tubes ($\Lambda \sim 64/Re$) in the laminar flow regime. A weak decrease of the slope can be noticed on Fig. 7 whereas Reynolds number is far below the classical flow regime transition around $Re = 2300$ for straight channel. To illustrate this low Reynolds number flow regime transition, Fig. 8 shows the evolution of the Darcy coefficient in the SAR-1 channel on a wider Reynolds number range.

As observed in Fig. 7, the linear sharp decrease is measured for Reynolds number ranging from 10 to around 100. Above 100, the transitional zone seems to appear and finally a moderate slope is observed for higher Reynolds numbers. These trends are similar to straight channels except that the transitional zone in our geometry is around $Re = 100$ rather than $Re = 2300$. Flow instabilities above these Reynolds number may certainly promote turbulence-like vortices. This is interesting to promote heat and mass transfer intensification while working with low Reynolds numbers. Similar trends have been observed by Theron et al. [6] in the corrugated channel.

In the low Reynolds number zone, Fig. 7 shows discrepancies between the SAR patterns. Losses in the SAR-3 geometry are higher than in SAR-1 and SAR-2 geometries (up to $\times 2$). This may be due to the number of patterns per developed length unit which is around 50% higher in SAR-3 than in SAR-1 and 2 (39.5 vs 25 patterns/ L_{dev}). The fluid undergoes a higher number of splitting and recombination which produces losses. Moreover, the ratio between the length of the branches where the fluid flows with a velocity $u/2$ and the

Table 2
Physico-chemical properties of the fluids used for pressure drop measurements.

| Fluid | Density ρ (kg m ⁻³) | Viscosity μ (Pa s) | Flowrate F_p (kg h ⁻¹) | Reynolds, Re |
|------------------------------------------------|--------------------------------------|------------------------|--------------------------------------|--------------|
| Water – Glycerol (70% weight glyc.) | 1030 | 0.018 | 1.4–18.0 | 5.3–110.9 |
| Water – Glycerol (90% weight glyc.) | 1015 | 0.210 | 0.3–7.1 | 0.1–3.3 |
| Water –Ethylene glycol (98% weight eth. Glyc.) | 1110 | 0.010 | 1.0–27.5 | 9.0–316.0 |

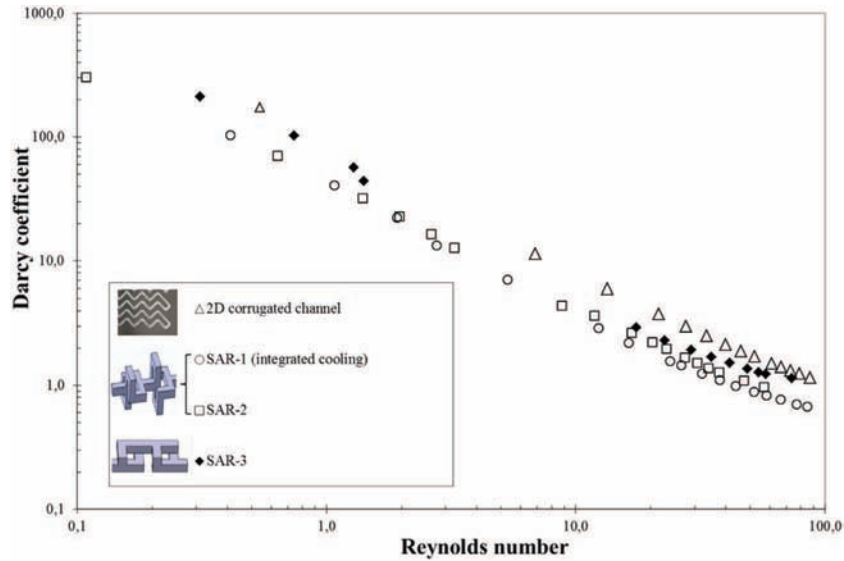


Fig. 7. Darcy coefficient vs Reynolds number (glycerol 70% and glycerol 90% at 25 °C).

developed length is lower in SAR-3 than in SAR-1 and 2. The pressure drop is directly proportional to the square of the velocity and this also generates additional losses in SAR-3 pattern.

The slight discrepancy between SAR-1 and SAR-2 curves might be explained as well since SAR-1 geometry has been expanded compared with SAR-2. This means that the length of one SAR-1 pattern is slightly higher than the one of the SAR-2 pattern, i.e. the fluid undergoes a little bit less splitting and recombination per unit of developed length (29 vs 25 patterns/ L_{dev}).

Finally, the corrugated channel generates higher losses than SAR geometries in the low Reynolds number range ($Re < 100$). The chaotic structures seem to generate moderate losses compared to the turbulent-like structures of the corrugated geometry.

3.2. Thermal characterization

3.2.1. Experimental set-up and procedure

The HEX reactors are equipped with temperature sensors to characterize the temperature profiles versus the flow regime. The temperature is measured between the inlet and outlet of each row

(see Figs. 4 and 5). Either a counter-current flow (SAR-2, SAR-3) or a cross-flow (SAR-1, corrugated channel) pattern is implemented for the cooling stream. The intermediate temperature probes are required to locate the temperature pinch and to avoid underestimating the heat transfer capacity.

To characterize the thermal behaviour of the HEX reactors, a heat transfer capacity, or thermal intensification factor, UA/V ($kW K^{-1} m^{-3}$), is assessed. U is the global heat transfer coefficient ($W m^{-2} K^{-1}$), A is the heat exchanger area (m^2) and V is the volume of fluid (m^3).

In both the SAR patterns and the 2D corrugated geometry, the heat exchange area can be defined according to various references. It can represent the developed heat exchange area of the 4 faces of the channel, or a projected area (i.e. assuming no heat transfer limitations in the process plate material). The 3-dimensions characteristic of the SAR structures add an extra level of complexity and the results in terms of heat transfer coefficient (and the resultant Nusselt number) depends on the chosen reference. It may lead to interpretation mistakes when the HEX reactors are compared.

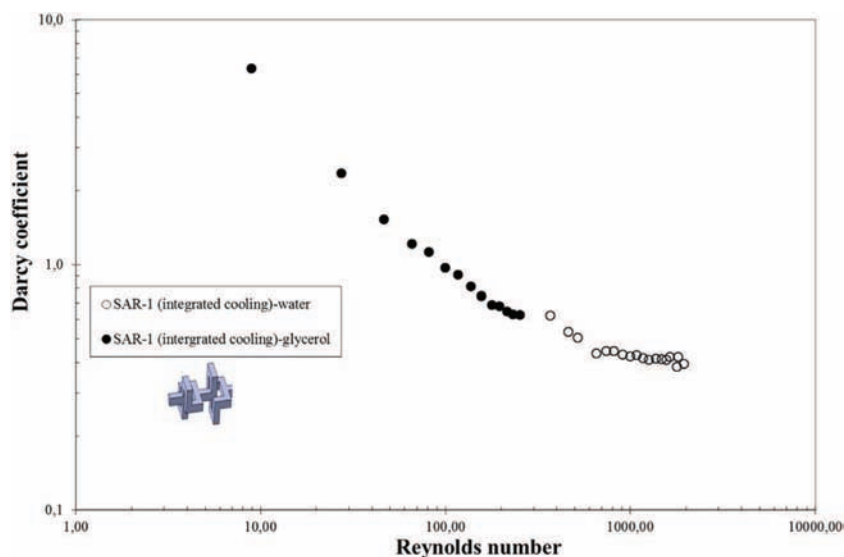


Fig. 8. Evolution of the Darcy coefficient vs Reynolds number in the SAR-1 channel (Water and ethylene glycol – 25 °C).

The thermal intensification factor is thus directly assessed from temperature measurements and no heat exchange area reference is required:

$$U \cdot A = \frac{P_{th}}{\Delta T_{ml}} \quad (3)$$

where P_{th} (W) is the exchanged power between the process fluid and the cooling fluid:

$$P_{th} = F_p \cdot C_p \cdot (T_{p,in} - T_{p,1}) \quad (4)$$

and ΔT_{ml} is the logarithmic mean temperature:

$$\Delta T_{ml} = \frac{(T_{p,in} - T_{u,out}) - (T_{p,1} - T_{u,in})}{\ln\left(\frac{T_{p,in} - T_{u,out}}{T_{p,1} - T_{u,in}}\right)} \quad (5)$$

$T_{p,in}$ as well as $T_{u,in}$ are the inlet temperatures of process and cooling (also named utility) fluids respectively. $T_{p,1}$ is the temperature measured at the first temperature sensor connection. $T_{u,out}$ is the outlet temperature of the utility stream.

3.2.2. Results and discussion

Fig. 9 displays the heat transfer capacity as a function of the Reynolds number for the three SAR heat exchanger/reactors.

The behaviour of the three SAR geometries is clearly distinct. The high ratio of splitting and recombination per unit of length of SAR-3 geometry (+50% compared with SAR-1 and SAR-2 geometries) seems clearly to favour heat transfer. Despite a small difference between the number of pattern per unit of length in SAR-1 and SAR-2 geometries, respectively 25 pattern/ L_{dev} and 29 pattern/ L_{dev} , an increase of the heat transfer capacity up to 30% is measured in SAR-2 heat exchanger reactor. To integrate the 22 cooling tubes through the SAR-1 channel in a cross-flow configuration, their diameter is limited (2 mm). Because of high pressure drops, this limits the utility flowrate. The contribution of the utility stream thermal resistance may be no longer negligible in the global heat transfer assessment as it is for the plate-type cooling (SAR-2 configuration). As a consequence, the increase of the process flowrate in SAR-1 channel does not contribute directly to the increase of the heat transfer capacity. This emphasizes the difference between SAR-1 and SAR-2 geometries, especially when the Reynolds number increases above $Re = 200$.

Above $Re = 150$, the slope of the SAR-3 curve diminishes and heat transfer capacity of SAR-2 configuration becomes higher. For

such Reynolds number, advection may become the most dominant phenomena (over diffusion) and the flow is mainly governed by secondary and Dean vortices. Heat transfer then depends on the number of 90° bends per unit of developed length which is higher in the SAR-2 pattern than in the SAR-3 one (respectively 173 bends/m vs 118 bends/m).

Fig. 10 illustrates the effect of fluid viscosity. The heat transfer capacity is plotted as a function of the Reynolds number for a more viscous fluid ($Pr \sim 200$).

It is consistent with results displayed in Fig. 9 below $Re = 150$. For low Reynolds number, advection is no more the dominant flow mechanism and a balance is made between advection and diffusion. As a consequence, the number of SAR patterns/ L_{dev} influences the heat transfer capacity.

3.2.3. Comparison with the 2D corrugated geometry

Fig. 11 compares the heat transfer capacity of each HEX reactor (both SAR geometries and 2D corrugated one) as a function of the energy dissipation rate ε ($W m^{-3}$). This parameter represents the required pumping power and is defined as:

$$\varepsilon = \frac{F_p \cdot \Delta P}{\rho \cdot V} \quad (6)$$

Above $1000 W m^{-3}$, the heat transfer capacity of the 2D corrugated channel is clearly higher than the one of the SAR geometries. It corresponds to Reynolds number around 100. As observed in Fig. 9, the flow is governed by advection and Dean vortices allow the intensification of heat transfer while generating moderate friction losses.

Below $1000 W m^{-3}$, heat transfer capacities are similar in function of the energy dissipation rate whatever the flow pattern. This is an interesting result considering both mixing and heat transfer capacity. Indeed, Ghanem et al. [23] showed that the SAR geometries promote mixing when compared to 2D corrugated geometry and Fig. 11 shows that heat transfer in SAR patterns can compete with corrugated channel performances. We can conclude that they are good candidate for chemical synthesis implementation with viscous fluids.

The Fig. 12 illustrates the effect of Prandtl number on the thermal and hydraulic performances of the structured flows. The exchanged thermal power to the pumping power ratio is plotted. It is function of the geometry, the Prandtl number and the Reynolds number.

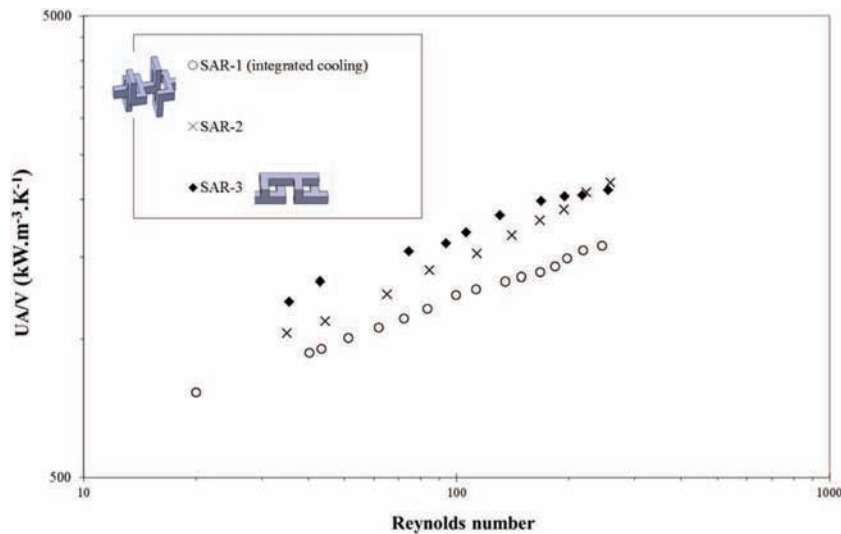


Fig. 9. Heat transfer capacity vs Reynolds number (glycerol 70% weight – $Pr \sim 40$).

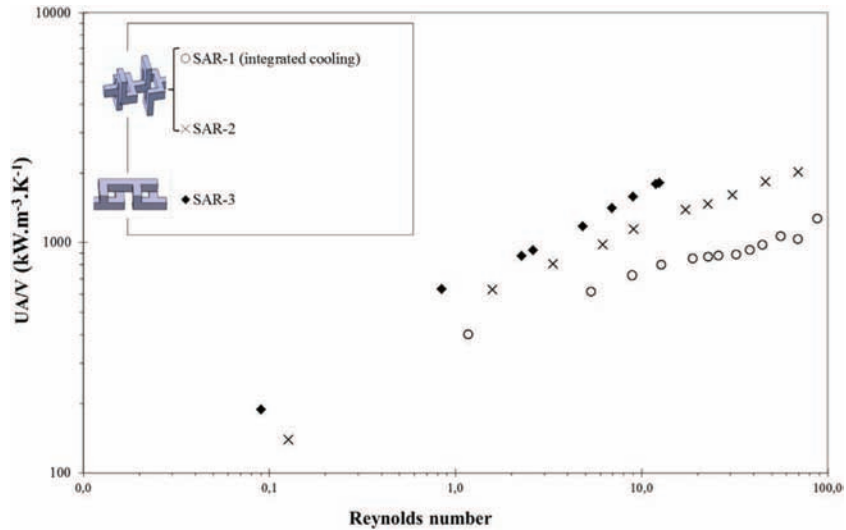


Fig. 10. Heat transfer capacity vs Reynolds number (glycerol 90% weight – Pr ~ 200).

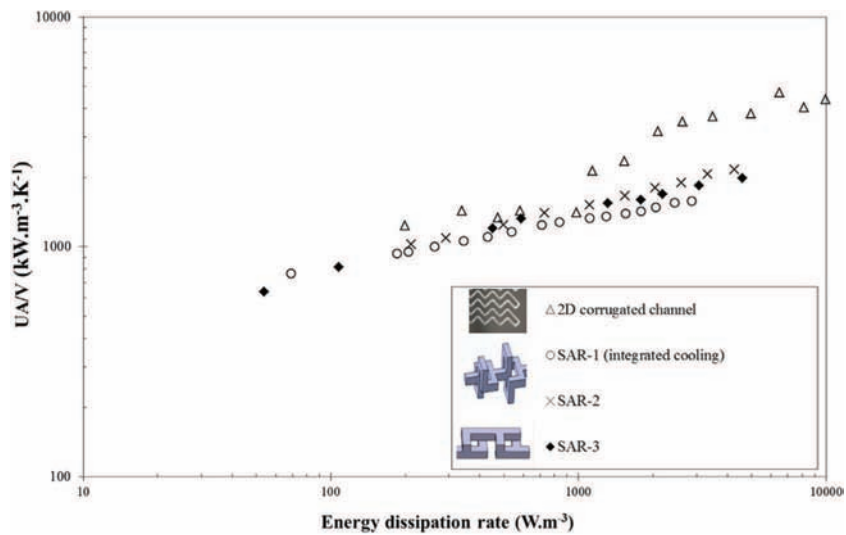


Fig. 11. Heat transfer capacity vs. energy dissipation rate (glycerol – 70% weight).

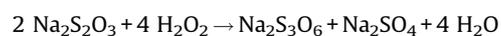
Fig. 12 shows that whatever the geometry and the fluid, the P_{th}/ε ratio decreases when the Reynolds number increases. This means that the heat transfer intensification regarding energy saving is more significant at lower flow regime. When SAR and corrugated geometries are compared, two behaviours are observed depending on the Prandtl number. For low Prandtl number (water), the power ratio is higher in the corrugated channel than in the SAR patterns (x2) whereas for high Prandtl numbers (glycerol 70%w.) power ratios are similar. In our case, the increase in Prandtl number favours the diffusion effect vs advection. As a consequence, advection which appears as the predominant phenomenon and seems to govern the water flow (low Prandtl number) favours the power ratio in the 2D corrugated geometry compared with the SAR ones. When the viscosity increases, the balance between advection and diffusion effects is shifted and the SAR mechanism seems to become interesting over advection. SAR-3 pattern shows a lower power ratio than other geometries. This is consistent with results

displayed in Figs. 7 and 9, the higher heat transfer capacity (see Fig. 9) does not compensate the higher pressure drop (see Fig. 7).

4. Implementation of a case study – exothermal reaction

4.1. The oxidation reaction

Based on the promising results of the thermal characterization, an exothermic reaction is implemented in the SAR-1 HEX reactor. This is the oxidation of sodium thiosulfate $\text{Na}_2\text{S}_2\text{O}_3$ by hydrogen peroxide H_2O_2 :



This reaction occurs in homogeneous liquid phase, is irreversible, fast and its reaction heat is $\Delta H_r = -586.2 \text{ kJ mol}^{-1}$. Since it is temperature sensitive, i.e. the conversion rate depends on the

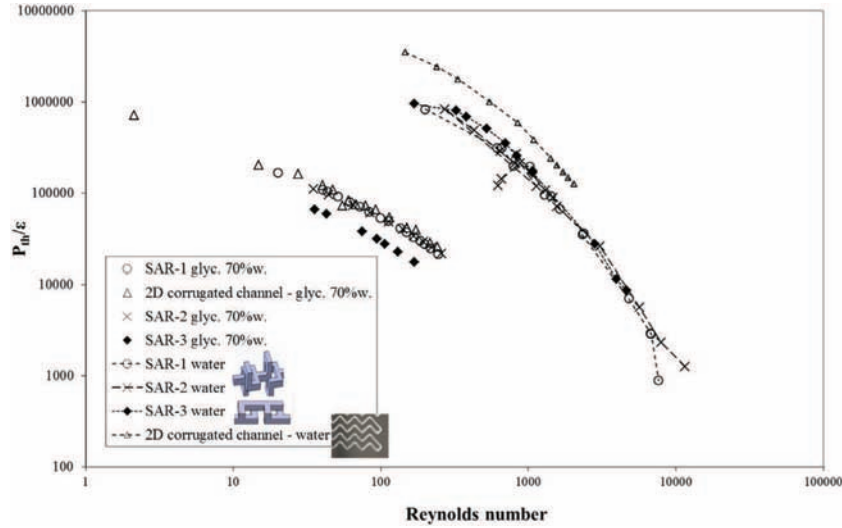


Fig. 12. Thermal exchanged power to pumping power ratio vs Reynolds number (glycerol 70% weight – $Pr \sim 40$ and water – $Pr \sim 7$).

operating temperature, this reaction is an ideal candidate for case study [4,24–28].

4.2. Experimental set-up

The implemented experimental set-up and procedure are similar to the ones described by Theron et al. [6]. The oxidation reaction involves two aqueous solutions of sodium thiosulfate and hydrogen peroxide as reactants. To avoid too high temperatures inside the reactor in case of an adiabatic rise the two solutions are both prepared in order to reach 9% in mass of each reactant in water. Two operating temperatures, controlled by the utility stream temperature, are tested: 40 and 50 °C. For these experiments the reactor is thermally insulated thanks to a polystyrene jacket.

The operating conditions are listed in Table 3.

The conversion rate χ in the reactor is deduced from the reactor thermal balance between the process and utility inlets and outlets at steady state. The conversion is thus calculated as follows:

$$\chi = \frac{P_{loss} + F_p \cdot C_{pp} \cdot (T_{p,out} - T_{p,in}) + F_u \cdot C_{pu} \cdot (T_{u,out} - T_{u,in})}{P_{reaction}} \quad (11)$$

where

F_p and F_u are the mass flowrate in respectively the process and the utility channels

$P_{reaction}$ is the total heat of reaction:

$$P_{reaction} = \dot{n}_i \cdot \Delta H_r \quad (12)$$

where \dot{n}_i is the initial molar flowrate of the limiting reactant ($\text{Na}_2\text{S}_2\text{O}_3$).

P_{loss} is the heat loss. It is measured from preliminary unreactive tests. Both the process and the utility lines are fed with water at the

temperatures and flowrates targeted for the reaction tests. The heat losses are assessed when steady state is reached.

4.3. Results and discussion

The measured conversion rates are given in Table 3 for each experiment.

As expected the conversion rate increases when increasing either the residence time in the reactor or the temperature of the utility stream. It is interesting to note that a utility temperature below 40 °C almost inhibits the reaction in the HEX reactor. As a consequence the minimal utility temperature of 40 °C allows the initiation of the reaction and then the control of the temperature rise due to the reaction exothermicity.

The Fig. 13 shows the conversion profile versus time obtained from the Grau et al. [29] kinetic law and the experimental data for both the 2D corrugated HEX reactor (see [6], $T = 42.9$ °C) and the SAR-1 one ($T = 47.5$ °C).

At fixed utility inlet temperature the different flowrates experimentally tested enable to compare the conversion to the kinetic data reported in the literature at different stages of the reaction.

The experimental data displayed in Fig. 13 are obtained with a utility temperature equal to 40 °C. The equilibrium temperature at the process outlet is higher in the SAR-1 HEX reactor (47.5 °C) than in the corrugated one (42.9 °C). This is consistent with the heat transfer characterisation (see Fig. 10) which showed that for inviscid fluid heat transfer capacity of the corrugated geometry is higher.

The Fig. 13 shows that for both conversion rates of 88 and 94% the kinetic model results fit well with the experimental data since the discrepancy is lower than 6%. A higher discrepancy (15%) is

Table 3

Operating conditions of the oxidation tests.

| No. exp. | Process side | | | | Utility side | Conversion rate (%) |
|----------|---------------------------------------------------|--------------------------------------------------------------|-----------------|--------------------|---------------------------|---------------------|
| | $F_{\text{H}_2\text{O}_2}$ (kg h^{-1}) | $F_{\text{Na}_2\text{S}_2\text{O}_3}$ (kg h^{-1}) | Reynolds number | Residence time (s) | T_{utility} (°C) | |
| 1 | 1.7 | 3.4 | 472 | 20 | 40 | 94 |
| 2 | 2.4 | 4.8 | 667 | 14 | 40 | 88 |
| 3 | 3.4 | 6.8 | 944 | 10 | 40 | 59 |
| 4 | 2.4 | 4.8 | 667 | 13 | 50 | 99 |

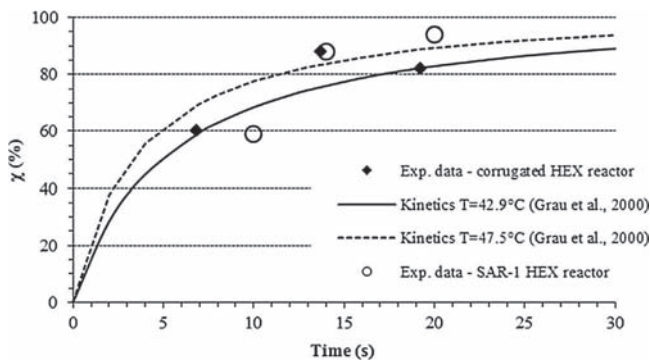


Fig. 13. Conversion rate vs. residence time ($T_u=40^\circ\text{C}$). Comparison of the theoretical conversion with the experimental ones.

obtained at the low residence time. The profile of conversion vs time obtained from Grau et al. data [29] assumes a constant temperature. However in the SAR HEX reactor, when the residence time decreases, i.e. when the flowrate increases, the temperature profile along the SAR channel is less uniform than for longer residence times. Almost 0.5 m, i.e. a quarter of the process channel developed length, is required to heat the reactant up to the desired temperature (40°C). In this part of the channel, the temperature is thus too low to initiate the reaction. As a consequence the effective residence time during which reactants are converted is shorter than the theoretical one reported in Fig. 13 ($F_p/V=10\text{s}$). This explains why the discrepancy between the conversion predicted from Grau et al. kinetics [29] and the measured one may increase when the flowrate increases.

However, the results obtained in this study show reasonable agreement with Grau et al. [29] kinetic parameters which have been obtained from batch experiments, especially for long residence time, i.e. low flowrates ($Re=573$ and 802). As a consequence it confirms that the mixing time is not a limiting parameter for such a fast reaction. Moreover, since heat transfer capacity in the SAR HEX reactor is high enough, the reaction can be implemented at higher temperature to accelerate the rate of reaction without safety issues.

5. Discussion/Conclusion

Thermal and hydraulic behaviour of a structured chaotic flow has been characterized in heat exchanger/reactors with channel designs based on Split-And-Recombine patterns. The principle is based on the Baker's transformation and chaotic structures are generated to promote heat and mass transfer intensification. Intensive mixing performances of such geometry have been demonstrated in previous studies [13,23] and this work investigated the energy efficiency of a heat exchanger/reactor integrating these SAR patterns.

Three stainless steel mock-ups –assembled by diffusion bonding- have been experimentally characterized. Two different flow patterns according to the number of SAR structures are available. For one of these geometries, two cooling systems have been investigated, external cooling Plates –isothermal wall- and integrated cooling tubes. For each mock-up, the 3 mm square cross-section channels are around 3.5 m long.

The SAR based reactors have been compared with a 2D corrugated geometry. The number of fluid splitting and recombination per unit of developed length is a design parameter promoting heat transfer but also generating higher friction losses. It results in similar performances considering the energy dissipation rate. Likewise, similar heat transfer capacities are measured between SAR-1 and SAR-2 geometries regardless of the cooling

system. The integrated cooling tubes system which is more complex to implement than the sandwiched plates seems not necessary.

According to the flow regime a balance between advection and diffusion exists. The former becomes predominant for high Reynolds number or low Prandtl number. Turbulent-like structures (like Dean vortices) appear and govern the transfer mechanisms. In these flow conditions, the design parameter seems to be the number of 90° bends/m and the corrugated geometry is much more performant. But when the fluid viscosity increases, the Split-And-Recombine mechanism seems to promote the chaotic nature of the flow and contributes with advection to the heat transfer intensification.

Considering the intensification of mixing in SAR geometries compared with corrugated one, maintaining high heat transfer at a similar level than the corrugated geometry is an interesting result regarding applications in chemical industry handling viscous fluids (food industry, bulk chemistry, polymers, ...). Implementing more viscous fluids could possibly help to completely dissociate the influence of advection versus diffusion.

A case study with the continuous oxidation of sodium thiosulfate with hydrogen peroxide has been studied. Conversions have been measured according to the cooling fluid temperature and the residence time. Conversions up to 99% have been reached with residence time around 13 s and confirmed that mixing time is not a limiting parameter for such a fast reaction. However this reaction involves inviscid fluids (viscosity close to water) and advection governs probably the flow. It could be interesting to complete these results with an exothermic reaction with viscous media.

Finally, SAR patterns could be candidate for scale-up procedure. When increasing the hydraulic diameter a balance between the increase of the Dean number (coupled to an increase of the losses) and the uniformity of the multi-laminated fluid stream should be the key issue.

References

- [1] A.I. Stankiewicz, J.A. Moulijn, Process intensification: transforming chemical engineering, *Chem. Eng. Prog.* 96 (2000) 22–34.
- [2] A. Cybulski, J.A. Moulijn, A.I. Stankiewicz, *Novel Concepts in Catalysis and Chemical Reactors: Improving the Efficiency for the Future*, Wiley-VCH, Weinheim, 2010.
- [3] Z. Anxionnaz, M. Cabassud, C. Gourdon, P. Tochon, Heat exchanger/reactors (HEX reactors): concepts technologies: state-of-the-art, *Chem. Eng. Proc.* 47 (2008) 2029–2050.
- [4] Z. Anxionnaz, M. Cabassud, C. Gourdon, P. Tochon, Transposition of an exothermic reaction from a batch reactor to an intensified one, *Heat Transfer Eng.* 31 (2010) 788–797.
- [5] Z. Anxionnaz-Minvielle, M. Cabassud, C. Gourdon, P. Tochon, Influence of the meandering channel geometry on the thermo-hydraulic performances of an intensified heat exchanger/reactor, *Chem. Eng. Process. Process Intensif.* 73 (2013) 67–80.
- [6] F. Theron, Z. Anxionnaz-Minvielle, M. Cabassud, C. Gourdon, P. Tochon, Characterization of the performances of an innovative heat-exchanger/reactor, *Chem. Eng. Process. Process Intensif.* 82 (2014) 30–41.
- [7] M. Moreau, N. Di Miceli Raimondi, N. Le Sauze, M. Cabassud, C. Gourdon, Pressure drop and axial dispersion in industrial millistructured heat exchange reactors, *Chem. Eng. Process. Process Intensif.* 95 (2015) 54–62.
- [8] A. Ghanem, C. Habchi, T. Lemenand, D. Della Valle, H. Peerhossaini, Mixing performances of swirl flow and corrugated channel reactors, *Chem. Eng. Res. Des.* 92 (2014) 2213–2222.
- [9] C. Habchi, S. Russeil, D. Bougeard, J.L. Harion, T. Lemenand, D. Della Valle, H. Peerhossaini, Enhancing heat transfer in vortex generator-type multifunctional heat exchangers, *App. Thermal Eng.* 38 (2012) 14–25.
- [10] European Process Intensification Center, EUROPIEC, <http://europic-centre.eu/>, 2016 (accessed 02.29.2016).
- [11] P. Carrière, On a three-dimensional implementation of the Baker's transformation, *Phys. Fluids* 19 (2007) 118110.
- [12] F. Raynal, P. Carrière, The distribution of time of flight in three dimensional stationary chaotic advection, *Phys. Fluids* 27 (2015) 1.4918750.
- [13] F. Schönfeld, V. Hessel, C. Hofmann, An optimised split-and-recombine micro-mixer with uniform 'chaotic' mixing, *Lab Chip—Miniat. Chem. Biol.* 4 (2004) 65–69.

- [14] B.L. Gray, D. Jaeggi, N.J. Mourlas, B.P. van Drieënhuizen, K.R. Williams, N.I. Maluf, G.T.A. Kovacs, Novel interconnection technologies for integrated microfluidic systems, *Sens. Actuators A Phys.* 77 (1999) 57–65.
- [15] H. Chen, J.-S. Meiners, Topologic mixing on a microfluidic chip, *Appl. Phys. Lett.* 84 (2004) 2193–2195.
- [16] J. Branebjerg, P. Gravesen, J.P. Krog, C.R. Nielsen, Fast mixing by lamination, *Proc. IEEE Micro Electro Mech. Syst. (MEMS)* (1996) 441–446.
- [17] M. Creyssels, S. Prigent, Y. Zhou, X. Jianjin, C. Nicot, P. Carrière, Laminar heat transfer in the MLLM static mixer, *Int. J. Heat Mass Transfer* 81 (2015) 774–783.
- [18] A. Ghanem, T. Lemenand, D. Della Valle, H. Peerhossaini, Optimized chaotic heat exchanger configurations for process industry: a numerical study, *Proc. ASME Fluids Eng. Div. Summer Meet.* (2013), Incline Village, USA.
- [19] A. Mokrani, C. Castelain, H. Peerhossaini, The effects of chaotic advection on heat transfer, *Int. J. Heat Mass Transfer* 40 (1997) 3089–3104.
- [20] C. Chagny, C. Castelain, H. Peerhossaini, Chaotic heat transfer for heat exchanger design and comparison with a regular regime for a large range of Reynolds numbers, *Appl. Therm. Eng.* 20 (2000) 1615–1648.
- [21] V. Kumar, S. Saini, M. Sharma, K.D.P. Nigam, Pressure drop and heat transfer study in tube-in-tube helical heat exchanger, *Chem. Eng. Sci.* 61 (2006) 4403–4416.
- [22] R. Couturier, C. Bernard, J.M. Leibold, F. Vidotto, P. Tochon, Device forming a chemical reactor with improved efficiency, comprising a heat exchanging circuit, Patent no WO 201 1/083 163 A1, 2011.
- [23] A. Ghanem, T. Lemenand, D. Della Valle, H. Peerhossaini, Transport phenomena in passively manipulated chaotic flows: Split-and-recombine reactors, *Proc. ASME Fluids Eng. Div. Summer Meet.* (2013), Incline Village, USA.
- [24] L. Prat, A. Devatine, P. Cognet, M. Cabassud, C. Gourdon, S. Elgue, F. Chopard, Performance evaluation of a novel concept “open plate reactor” applied to highly exothermic reactions, *Chem. Eng. Technol.* 28 (9) (2005) 1028–1034.
- [25] M.D. Grau, J.M. Nougues, L. Puigjaner, Batch and semibatch reactor performance for an exothermic reaction, *Chem. Eng. Proc.* 39 (2000) 141–148.
- [26] A.M. Benkouider, J.C. Buvat, J.M. Cosmao, A. Saboni, Fault detection in semi-batch reactor using the EKF and statistical method, *J. Loss Prev. Process Ind.* 22 (2009) 153–161.
- [27] L. Vernieres-Hassimi, M.A. Abdelghani-Idrissi, D. Seguin, Experimental and theoretical steady state maximum temperature localization along an exothermic tubular reactor, *Open Chem. Eng. J.* 2 (2008) 57–65.
- [28] W. Benaissa, S. Elgue, N. Gabas, M. Cabassud, D. Carson, M. Demissy, Dynamic behaviour of a continuous heat exchanger/reactor after flow failure, *Int. J., Chem. React. Eng.* 6 (2008).
- [29] M.D. Grau, J.M. Nougues, L. Puigjaner, Batch and semibatch reactor performance for an exothermic reaction, *Chem. Eng. Proc.* 39 (2000) 141–148.